Influence of temperature on passive film properties on Ni–Cr–Mo Alloy C-2000

Xiangrong Zhang [a], David W. Shoesmith [a,b,*]

[a] Department of Chemistry, University of Western Ontario, London, Ontario N6A 5B7, Canada
[b] Surface Science Western, University of Western Ontario, London, Ontario N6G 0J3, Canada

ABSTRACT

The properties of the passive film on a Ni–Cr–Mo alloy, Alloy C-2000 (Ni–23Cr–16Mo–1.6Cu), grown at various temperatures, were investigated by AR-XPS and ToF-SIMS. The presence of a layered structure in the passive film has been demonstrated at low and mild temperatures in neutral solutions, with an inner Cr_2O_3 layer, outer Cr/Ni hydroxides layer and Mo/Cu oxide in the outermost surface. As temperature increases, the thickness of both layers increase which improves passivity. Increasing temperature leads to a loss of Cr_2O_3 from the inner and of Mo/Cu from outer layers. These compensating effects make the passive current density almost independent of temperature.

© 2013 Elsevier Ltd. All rights reserved.

1. Introduction

Ni–Cr–Mo alloys exhibit exceptional corrosion resistance under extreme exposure conditions and are used in a range of industrial applications [1]. This resistance is generally attributed to the formation of a very stable passive film [2–6] whose compositional and electrical properties have been investigated using surface analytical methods [7–11] and electrochemical impedance spectroscopy (EIS) [3–5,12–17].

Lloyd et al. [7–9] determined the film composition and thickness and the effect of the alloying elements, Cr, Mo and W, on the passivity of a number of Ni–Cr–Mo (W) alloys in acidic solution. The oxide consists of a Mo, Cr, Ni oxide, with Cr present as Cr (III) and Mo in several oxidation states. The film was found to be only a few nanometers thick (<5 nm) and the thickness increased with increasing potential in the passive region. Time of Flight Secondary Ion Mass Spectrometry (ToF-SIMS) and X-ray Photoelectron Spectroscopy (XPS) showed the high-Cr alloys were able to build thicker oxides with a layered structure consisting of an inner Cr–Ni oxide and an outer Mo/W oxide when anodically oxidized in 1.0 M NaCl + 0.1 M Na_2SO_4 (pH 1). More recently, we have shown that a similar bilayer film is formed on Alloys C-22 and C-2000 in neutral solutions [10,11].

The variation in oxide electrical properties has been studied in detail. MacDonald et al. [14] characterized the oxide properties

on Alloy C-22 by EIS over the potential range from −0.2 to 0.7 V (vs. Ag/AgCl in saturated KCl). The interfacial impedance (expressed as the polarization resistance (R_p)) under extreme conditions (e.g., pH 3, saturated NaCl, 80 °C) was of the order of $10^5 \, \Omega \, cm^2$, indicative of a high corrosion resistance. R_p initially increased with applied potential due to the growth of the passive layer. At a sufficiently high potential ($E > 0.2$ V (vs. Ag/AgCl in saturated KCl)), which is close to the initiation of the transpassive state, R_p is observed to decrease with potential. This decrease was attributed to a thinning of the film.

More recently, Jakupi et al. [18] characterized the oxide film properties on Alloy C-22 by combining EIS and XPS measurements in near neutral pH, 5 M NaCl solutions at 30 °C. A similar variation in film resistance (R_{film}) with applied potential was observed. For the range $-0.6 \, V \leqslant E \leqslant -0.3 \, V$ (vs. Ag/AgCl in saturated KCl), R_{film} increased with potential accompanied by an increase in Cr (III) oxide content. Over the range $-0.3 \, V \leqslant E \leqslant 0.3 \, V$ (vs. Ag/AgCl in saturated KCl), R_{film} values and the Cr (III) oxide content achieved their maximum values. For $E > 0.3$ V (vs. Ag/AgCl in saturated KCl), a decrease in both R_{film} and the Cr (III) oxide content was observed.

Our interest in these alloys is primarily focused on their crevice corrosion behavior, a potential failure process if one of these alloys were to be used in the fabrication of nuclear waste containers [19]. This potential application has stimulated extensive study of the crevice corrosion of Alloy C-22, and to a lesser degree other Ni–Cr–Mo alloys [18,20–39]. Published studies show that the initiation of crevice corrosion is difficult [37] and even when forced to occur electrochemically is limited to minor damage [35,38,39].

* Corresponding author at: Department of Chemistry, University of Western Ontario, London, Ontario N6A 5B7, Canada.
E-mail address: dwshoesm@uwo.ca (D.W. Shoesmith).

Using a combination of electrochemical techniques, Raman Spectroscopy and Confocal Scanning Laser Microscopy (CSLM) [38], it was demonstrated that crevice propagation was limited by one, or a combination, of the following processes; (i) inhibited O_2 reduction kinetics on passive surfaces external to the crevice; (ii) the rapid accumulation of molybdates at activated locations within the crevice.

These studies raise the question of whether conditions sufficiently aggressive to initiate and support the propagation of crevice corrosion can be established. In this paper, we investigate the influence of increasing temperature on passive film properties, a feature which would be expected to destabilize the film and increase the probability of crevice initiation.

The effect of temperature on the passive behavior of Ni–Cr–Mo alloys has been studied by a number of researchers. Ashida et al. [40] investigated the effect of temperature on Alloy C-22 in simulated groundwater (pH 9.8) using a temperature-oscillating heated electrode technique. The corrosion potential (E_{corr}) was found to increase linearly from −0.293 V to −0.256 V (vs. Ag/AgCl in 3.5 mol/L KCl) when the temperature decreased from 103 °C to 72 °C, and the passive current density to increase exponentially over the temperature range 65 °C to 95 °C. Evans and Rebak [41] observed a similar exponential relationship between passive corrosion rate and temperature (30 °C to 90 °C) on the same alloy in both deaerated and aerated simulated acidified water (pH 2.8). Gray et al. [3], however, found the corrosion rate to be independent of temperature below 50 °C, and then to increase approximately linearly between 50 °C and 90 °C in H_2SO_4 and HCl. This behavior was ascribed to either an increase in solubility of Cr or to a phase change in the passive layer around 50 °C. In a comparison of a number of Ni–Cr–Mo alloys, Lloyd et al. [7] found the temperature dependence of the passive current on Alloy C-22 to be significantly less than that for Alloy C-276 due to the lower oxide dissolution rate compared to the rate of creation of oxygen vacancies leading to film growth. A possible reason for these inconsistencies in behavior is differences in pretreatment of the alloy, the establishment of a steady-state passive condition requiring a few days at least after surface preparation and immersion of the alloy.

Despite these efforts the influence of temperature on the passive film composition and structure are poorly characterized. In this paper, we have used Angle Resolved XPS (AR-XPS) and ToF-SIMS to investigate the changes in oxide film composition as a function of temperature up to 90 °C.

2. Experimental

2.1. Materials and electrode preparation

Cylindrical specimens were cut from plate materials supplied by Haynes International, Kokomo, Indiana (USA), with a diameter of 1 cm and a height of 0.5 – 1 cm. The cylinders were drilled at one end to allow electrical connection to a threaded rod of the same material. Prior to each experiment, the surface of each specimen, with a surface area of 0.785 cm^2, was wet-ground with a series of SiC papers up to 1200 grit, and then polished successively with 5.0, 0.3, and 0.05 μm alumina powder suspensions. Specimens were then swabbed with cotton under running water to reduce the chances of staining, and finally rinsed with large amounts of Type 1 water obtained from a Milli-Q Academic A-10 system. Specimens were immersed first in acetone and then in Type 1 water and ultrasonicated for 10 min to remove any attached polishing residue, rinsed again with large amounts of Type 1 water, and immediately placed in the electrochemical cell to grow the oxide film.

2.2. Electrochemical film growth

A standard three-electrode, glass electrochemical cell housed in a grounded Faraday cage was used. The cell contains a working electrode (WE), a pure platinum (99.95% purity) counter electrode (CE) and an in-house fabricated silver/silver chloride (Ag/AgCl) reference electrode (RE) in saturated KCl solution (199 mV vs. SHE at 25 °C). The cell was fitted with an outer jacket through which silicon oil or water was circulated from a thermostatic bath (Isotemp 3016H, Fisher Scientific) to maintain the temperature of the solution to within ±1 °C.

Freshly-prepared 5 M NaCl solutions were used as the electrolyte. The solutions were prepared from reagent grade NaCl and Type 1 water. Prior to starting each experiment, the electrolyte solution was purged for at least 1 h in UHP argon (Praxair) and purging continued throughout the experiment.

A Solartron 1284 multistat was used to apply a constant potential to the electrode, half-immersed in a stirred electrolyte. A period of 60 min of cathodic cleaning at −1.0 V (vs. Ag/AgCl in saturated KCl) was required to guarantee a reproducible surface. Over this time the cathodic current achieved a constant and reproducible value. Once this value was achieved it was presumed that a reproducibly defective Cr oxide/hydroxide layer was present and that the current was completely due to water reduction. Subsequently, a film formation potential was applied for 44 h to grow an oxide film, and Corrware software (Scribner Associates) was used to record the data. The potentials applied were 0 V (vs. Ag/AgCl in saturated KCl) to grow the passive film [18]. Experiments were performed at either room temperature (22 °C), 50 °C or 90 °C.

After film-growth, the specimen was immediately removed from the cell, rinsed and ultrasonicated for 2 min in Type 1 water (at the same temperature as the solution in the cell) to remove any electrolyte left on the specimen surface. The specimen surface was then dried in a stream of argon gas, placed in a small tin box and stored in a desiccator. Subsequently, the specimen was analyzed using AR-XPS and ToF-SIMS. The reliability of these analyses has been discussed previously [10].

2.3. Surface analyses

All AR-XPS analyses were carried out with a Kratos Axis Ultra spectrometer at Surface Science Western using a monochromatic Al Kα (1486.6 eV) source. The instrument work function was calibrated to give an Au 4f$_{7/2}$ metallic gold binding energy of 83.95 eV. The spectrometer dispersion was adjusted to give a binding energy of 932.63 eV for metallic Cu 2p$_{3/2}$. The Kratos charge neutralizer system was used for all the analyses. The apparent shifts of the spectra were calibrated using the C 1s peak set to 284.8 eV. High-resolution spectra were obtained using a 20 eV pass energy, whereas survey spectra were recorded using a 160 eV pass energy with an analysis area of ∼300 μm × 700 μm. Two photoelectron take-off angles (measured from the sample surface), 30° and 90°, were used to analyze the oxide film on Alloy C-2000. Analyses performed at the take-off angle of 30° probe shallower depths than those recorded at an angle of 90°. Based on the inelastic mean free paths for Ni and Cr oxides/hydroxides, a depth of 5 to 7 nm would be probed at a take off angle of 90° and a depth of 2 to 4 nm at the angle of 30° [42]. By comparison of the information obtained at a grazing take-off angle (30°) to that at an angle close to the surface normal (90°), information on the variation of composition with depth can be obtained.

An ION-ToF time-of-flight secondary ion mass spectrometer (ToF-SIMS IV) was used to obtain the ToF-SIMS depth profiles and cross-sectional images for sputtered specimens. A 1 keV Cs$^+$ ion beam was used to sputter an area of 200 × 200 μm^2 on the specimen and negative secondary ions were collected from a

100×100 μm^2 area within the sputter crater using a 25 keV monoisotopic Bi$_3^+$ primary ion beam. A smaller analysis area was used within the sputter crater dimensions to avoid edge effects. Each ToF-SIMS mass spectrum was calibrated using the exact mass values of at least 3 known species in the spectrum collected during profiling.

3. Results

3.1. Electrochemical behavior

Fig. 1 shows log- log plots of current transients recorded on Alloy C-2000 polarized at 0 V (vs. Ag/AgCl in saturated KCl) for 44 h at three temperatures (22, 50, 90 °C) in a neutral deoxygenated 5 M NaCl solution. This potential was chosen because the passive film is expected to be fully developed at this value [18]. For times $\leqslant 10^2$ s the current is almost independent of time at the two lower temperatures. This can be attributed to the change in composition and decrease in defect content of the cathodically-reduced air formed film remaining on the electrode surface after the cathodic pretreatment. For times $\geqslant 10^3$ s the current density decreases logarithmically with log time at all three temperatures, as expected for the solid state growth of a passive oxide [8,43]. After 44 h, while steady-state is not achieved, current densities in the region of 100–300 nA cm^{-2} are measured indicating the establishment of passivity. Although steady-state is not achieved after this period, it is sufficiently long to establish the chemical properties of the oxide film. A longer period of oxidation would be expected to change the composition only slightly while eliminating residual defects in the oxide. The currents are only slightly dependent on temperature.

3.2. Surface analyses

3.2.1. AR-XPS results

An example of a survey spectrum on this alloy is shown in Fig. 2. The surface compositions determined from XPS survey spectra at the three temperatures recorded at the two angles are shown in Fig. 3. As expected, the O signal is stronger at a take-off angle of 30° than 90° since the depth probed at the latter angle can penetrate into the alloy, Fig. 3(a). The O signal at both angles increases with temperature indicating an increase in film thickness with temperature. At 90 °C, the O signal at the two take-off angles approaches the same value as the substrate alloy becomes more difficult to detect beneath the thicker oxide film.
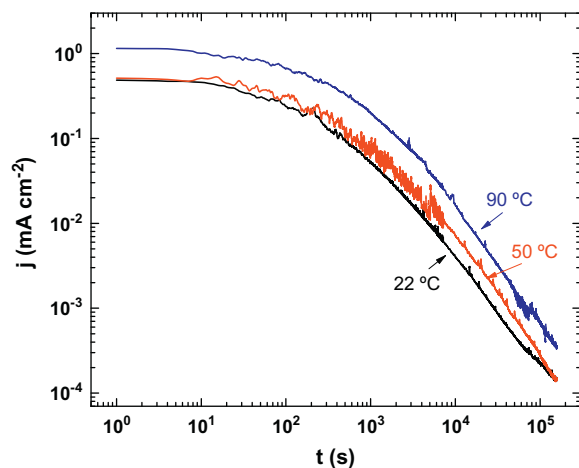

Fig. 1. Log current density (j) – log time (t) plots recorded on Alloy C-2000 polarized at 0 V (vs. Ag/AgCl in saturated KCl) at three temperatures (22, 50, and 90 °C) in neutral deoxygenated 5 M NaCl solution.
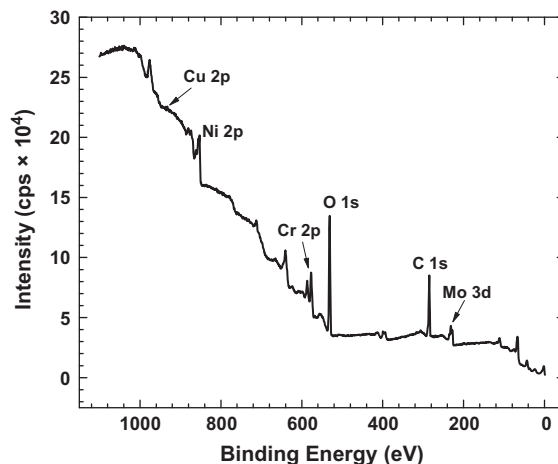

Fig. 2. XPS survey spectrum measured at the take-off angles of 90° recorded on an Alloy C-2000 surface after polarization at 0 V (vs. Ag/AgCl in saturated KCl) (pH 7, 44 h) at 22 °C.
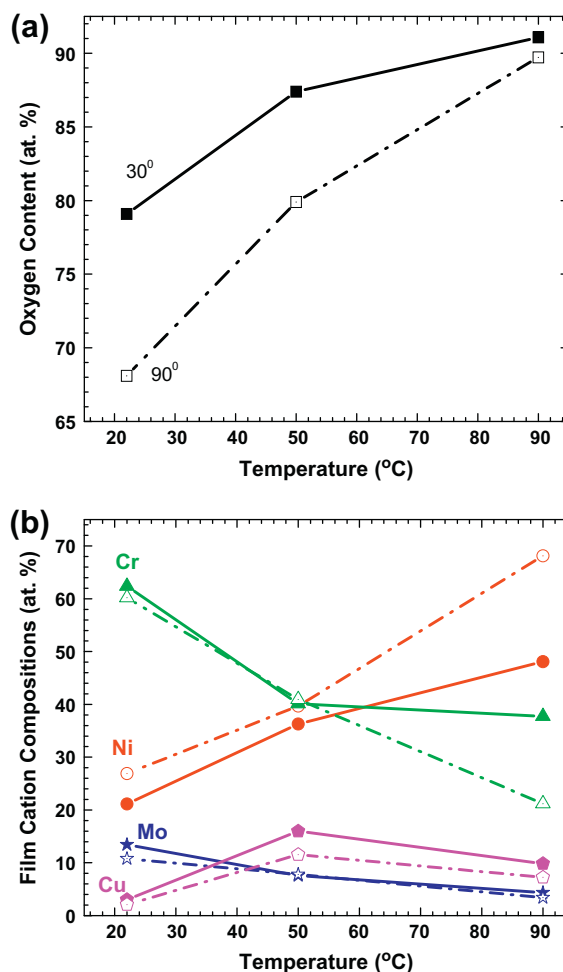

Fig. 3. Oxygen content (a) and film cation compositions (b) determined from the survey spectra measured at take-off angles of 30° (solid line) and 90° (dashed line) recorded on Alloy C-2000 after polarization at 0 V (vs. Ag/AgCl in saturated KCl) (pH 7, 44 h) at various temperatures. The latter is corrected for contributions from the metallic substrate determined from high-resolution spectra.

The cation composition of the film, corrected for contributions from the metallic substrate (determined from high resolution spectra) is shown as a function of temperature in Fig. 3(b). By

comparison to the composition of the substrate, Ni is depleted and Cr enriched in the oxide film, which is expected. With increasing temperature the Ni content of the film increases while the Cr and Mo contents decrease. The Cu content increases markedly over the range 22 °C to 50 °C before decreasing at 90 °C. At 22 °C Ni appears to be slightly enriched in the inner regions (i.e., the Ni content is greater at the take-off angle of 90° compared to 30°) and Mo in the outer regions of the film. The anticipated higher Cr content in the inner-barrier layer region of the film is not detected.

When the temperature is increased to 50 °C, changes in Ni and Cr distribution are marginal, the enhanced Mo content of the outer region disappears, and the segregation of Cu to the outer film is clearly observed. When the temperature is further increased to 90 °C only marginal changes in the distribution of Cu and Mo are observed while a significant redistribution of Ni and Cr occurs. The relative Ni and Cr contents of the inner and outer layers of the film increase, respectively. The overall decrease in Cr content of the film suggests a significant decrease in Cr content of the inner-barrier layer with temperature.

High resolution scans of the Ni2p, Cr2p, Mo3d, Cu2p, O1s and C1s regions of the spectrum were performed at all three temperatures and both take-off angles. As described previously [11], these spectra were deconvoluted after a Shirley background correction [44] using the peak parameter values published by Biesinger et al. (Ni [42,45], O [42], Cr [45,46]), and McIntyre et al. (Mo [47]). Examples of deconvoluted spectra have been published previously [11]. The relative amounts of the various species for each element obtained from such spectra at each temperature are shown in Fig. 4.

Fig. 4(a) shows that consistently higher OH and lower O contents are observed at the shallower take-off angle (30°) indicating

the outer region of the film is dominantly hydroxide and the inner region dominantly oxide. The change in OH and O contents from 22 °C to 50 °C indicates that, over this temperature range, the outer hydroxide grows at the expense of the inner oxide. At 90 °C, however, the increase in O at the expense of OH content at a take-off angle of 90° clearly demonstrates an overall increase in the inner oxide thickness. The overall increase in the total surface oxide/hydroxide thickness with temperature suggested by the results in Fig. 3(a) is confirmed by the decreased contribution of the metal signals for all three alloy components (Ni, Cr, Mo), Fig. 4(b–d).

Fig. 4(b) shows that the amount of $Ni(OH)_2$ is much higher, and that of NiO much lower, at the lower (30°) than the higher (90°) take-off angle demonstrating that the hydroxide is enriched in the outer regions compared to oxide in the inner regions of the film. The relative $Cr(OH)_3$ and Cr_2O_3 contents exhibit the same take-off angle dependence, Fig. 4(c). Comparison of the signals for both Ni and Cr, along with the observation that the Cr content of the film decreases relative to that of Ni (Fig. 3(b)) shows that the overall increase in the outer layer thickness over the temperature range 22 °C to 90 °C is attributable to the accumulation of Ni accompanied by the depletion of Cr.

The thickening of the inner layer oxide at 90 °C, Fig. 4(a), is confirmed by the increases in Ni (II) and Cr (III) oxide contents at a take-off angle of 90°, Fig. 4(b and c). That this increased thickness is predominantly due to Ni oxide formation is indicated by the results from the survey spectra, which show an increase in inner oxide Ni content at the expense of the Cr content.

Although a relatively minor component of the oxide/hydroxide film, the Mo oxidation states show significant changes with temperature and take-off angle. At the two lower temperatures, the relative amounts of Mo (VI) and Mo (V) are much higher at the
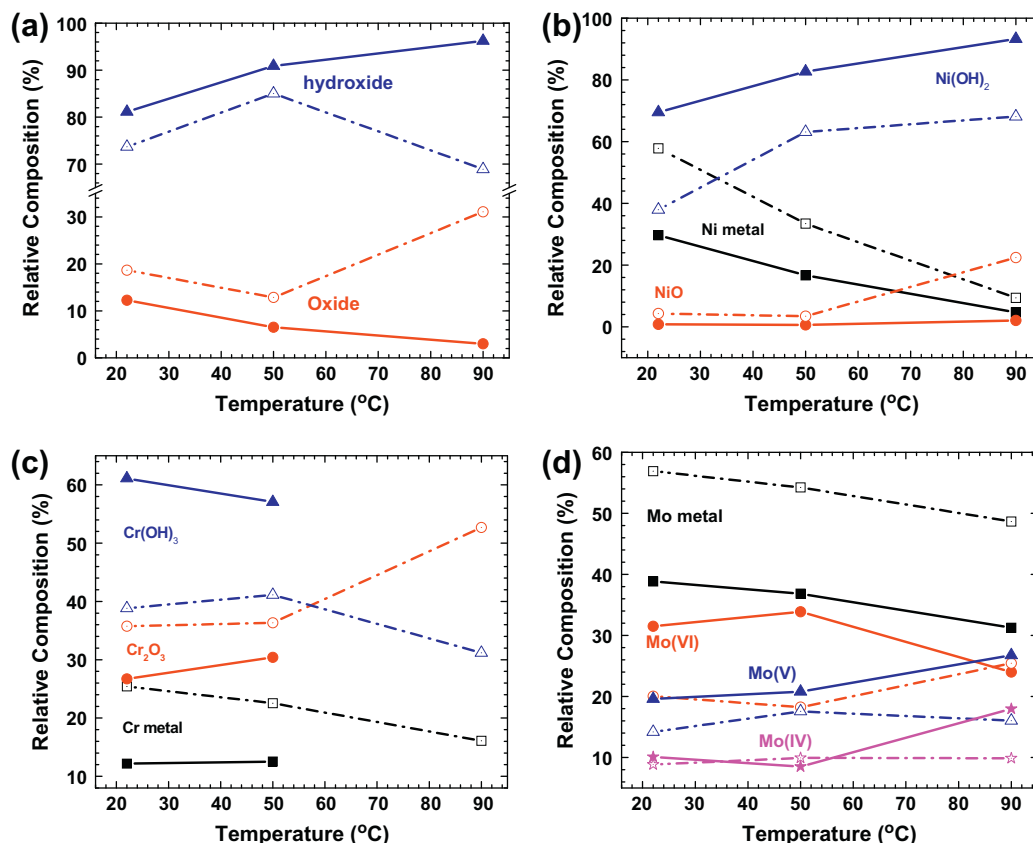

Fig. 4. Relative compositions of O (a), Ni (b), Cr (c), and Mo (d) species in the Alloy C-2000 surface after polarization at 0 V (vs. Ag/AgCl in saturated KCl) (pH 7, 44 h) measured at take-off angles of 30° (solid lines) and 90° (dashed lines) at various temperatures.
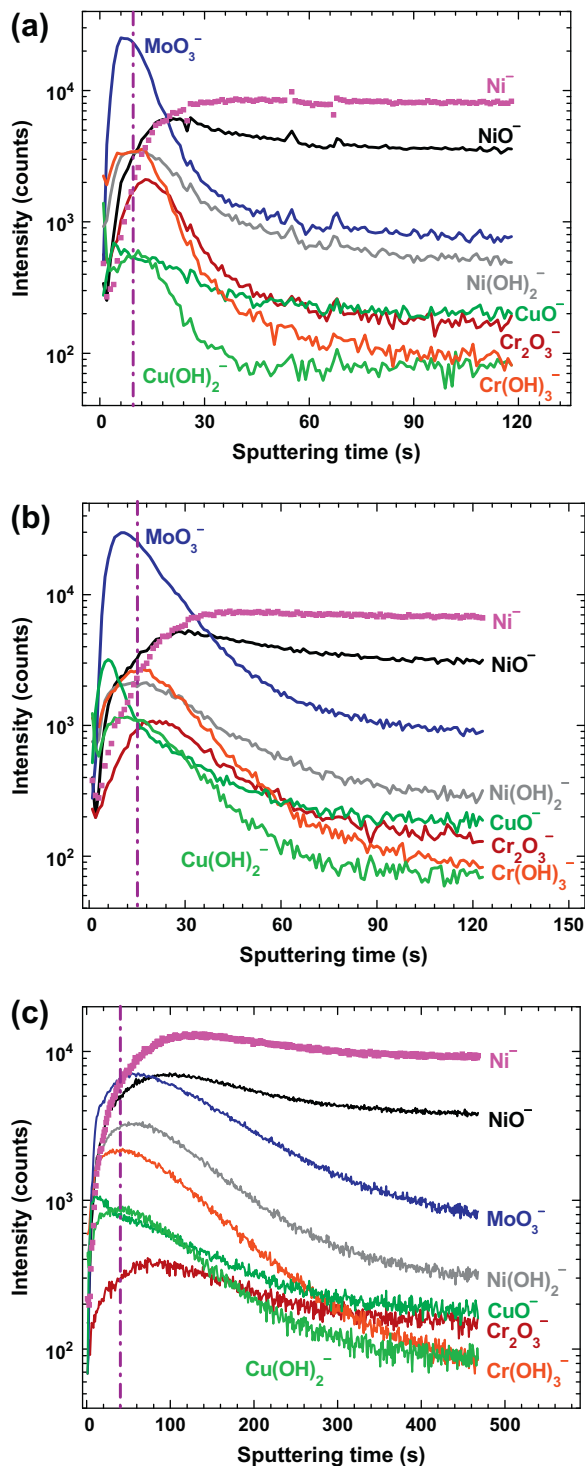
(a)

MoO₃⁻
Ni⁻
NiO⁻
Ni(OH)₂⁻
CuO⁻
Cr₂O₃⁻
Cu(OH)₂⁻
Cr(OH)₃⁻

Intensity (counts)
Sputtering time (s)

(b)

MoO₃⁻
Ni⁻
NiO⁻
Ni(OH)₂⁻
CuO⁻
Cr₂O₃⁻
Cu(OH)₂⁻
Cr(OH)₃⁻

Intensity (counts)
Sputtering time (s)

(c)

Ni⁻
NiO⁻
MoO₃⁻
Ni(OH)₂⁻
CuO⁻
Cr₂O₃⁻
Cu(OH)₂⁻
Cr(OH)₃⁻

Intensity (counts)
Sputtering time (s)

Fig. 5. ToF-SIMS profiles recorded on Alloy C-2000 after polarization at 0 V (vs. Ag/AgCl in saturated KCl) (pH 7, 44 h) at (a) room temperature (22 °C), (b) 50 °C and (c) 90 °C. The vertical dashed line represents the peak location of Cr(OH)₃⁻.

lower (30°) then the higher (90°) take-off angle showing an enrichment of the higher oxidation states in the outer regions of the film. However, at 90 °C, the relative percentage of Mo (VI) measured at the shallow take-off angle (30°) decreases significantly indicating this state is no longer enriched in the outer regions of the film. By contrast, despite the overall decrease in film Mo content, Fig. 3(b), the relative Mo (V) and Mo (IV) contents measured at the shallow take-off angle (30°) increase confirming their dominance in the outer regions of the film.

As observed previously [11], a single Cu 2p3/2 high-resolution peak with a binding energy ranging between 931.8 eV and 932.9 eV was observed. This is close to the binding energy for both Cu metal and Cu₂O, which are within 0.1 eV of each other and cannot be easily distinguished by XPS [48]. The satellite peak (5–10 eV higher on the binding energy scale than the principal Cu 2p3/2 line) indicative of the Cu (II) state was not observed.
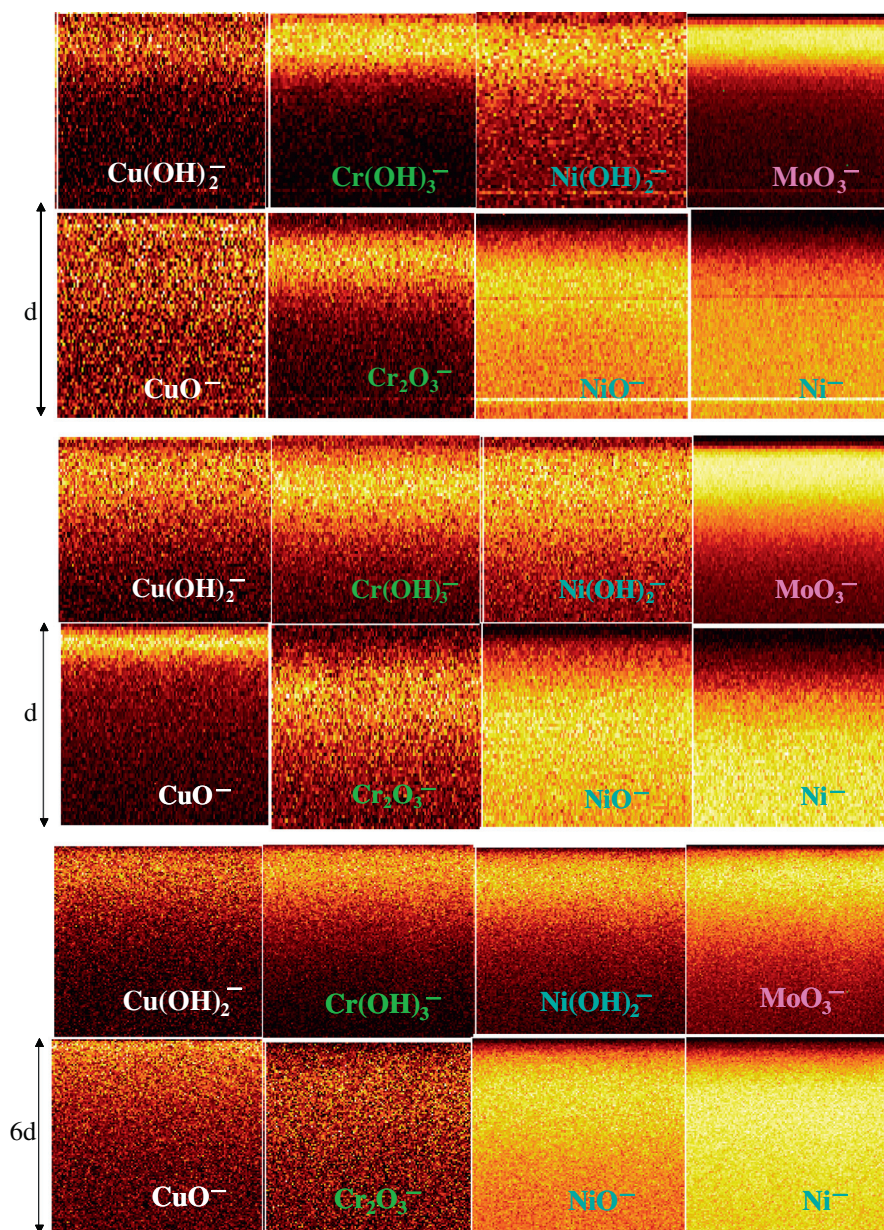
3.2.2. ToF-SIMS analyses

Fig. 5 shows the ToF-SIMS profiles for the negative ions detected, and Fig. 6 the cross-sectional images reconstructed from these sputtering profiles. Since the sputtering rates are unknown, these profiles cannot be converted to exact depth profiles. Also, since the negative ions detected in the spectra do not necessarily represent the species which exist in the oxide, the exact oxidation states of the ions cannot be determined. The sputtering profiles show that each species exhibits a maximum intensity at a specific time indicating its location within the film.

At the two lower temperatures the segregation of Cu and, to a lesser degree Mo, to the outer regions of the film is observed. This is particularly clear for Cu at 50 °C which is consistent with the XPS survey spectra results, Fig. 3(b). The hydroxides of Ni, Cr, and Cu are located at intermediate depths within the film and the inner barrier layer region is composed primarily of Ni and Cr oxides, with a strong enhancement of the latter compared to the Cr content of the substrate alloy. This layered structure is clearly shown in the cross-sectional images, Fig. 6, in which the lighter color indicates the location of individual species within the film. The slightly wider peaks in the sputtering profiles obtained at 50 °C, Fig. 5(b), compared to those obtained at 22 °C, Fig. 5(a), confirm the increase in film thickness with temperature and this is supported by the cross-sectional images, Fig. 6(a and b). This is most readily appreciated by comparing the widths of the light-colored panels (Fig. 6(a and b) for the MoO₃⁻ and Cr₂O₃⁻ ions at the two temperatures. Additionally, the peak for the CuO⁻ ion is more distinctly surface segregated at 50 °C compared to 22 °C, Figs. 5(a and b) and 6(a and b).

The compositional profiles, Fig. 5(c), and cross-sectional images, Fig. 6(c), confirm the major changes in film properties at 90 °C compared to the two lower temperatures. The significant difference in scale (sputtering time) confirms the large increase in film thickness indicated by the AR-XPS results. While Cu remains primarily in the surface layer it is no longer as distinctly segregated as at the two lower temperatures. Additionally, the loss of Cr (III) oxide from the inner regions of the film, the presence of Cr (III) hydroxide in the middle regions of the film, and the overall dominance of the film by its Ni content are also clear. The loss of Cr (III) from the inner barrier layer of the film as the temperature is increased is best exemplified by the Cr₂O₃⁻/MoO₃⁻ and Cr₂O₃⁻/CuO⁻ ratios obtained from the sputtering profiles, Fig. 7. The shorter sputtering time required to achieve a peak in the Cr₂O₃⁻/CuO⁻ ratio (indicated by the vertical dashed line) compared to that for Cr₂O₃⁻/MoO₃⁻ confirms the more emphatic surface segregation of Cu compared to Mo at the two lower temperatures. The very significant decreases in these two ratios and the disappearance of the peaks at 90 °C, confirm the loss of Cr (III) from the film consistent with the XPS results.

4. Discussion

The properties of passive oxide films on Alloy C-2000 have been studied as a function of temperature by AR-XPS and ToF-SIMS. The presence of a layered structure has been demonstrated previously and confirmed in this study [10,11]. The film comprises dominantly hydroxides in the outer layer and oxides in the inner layer. Cu and Mo segregate to the outer regions of the surface, leaving Cr
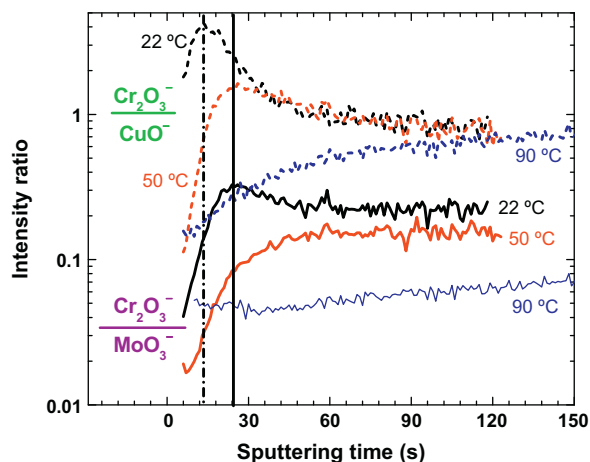
Fig. 6. ToF-SIMS cross-sectional images for Alloy C-2000 reconstructed from sputtering profiles after polarization at 0 V (vs. Ag/AgCl in saturated KCl) (pH 7, 44 h) at (a) room temperature (22 °C), (b) 50 °C and (c) 90 °C. The lighter colors indicate a higher content of the species shown in the images.

(and Ni) oxides enriched at the alloy/oxide interface. This segregation of Cr/Mo yields the bipolar film structure, consistent with observations on Mo-containing stainless steels [49] and on Ni–Cr–Mo alloys in acidic sulphate solution [8]. It has been claimed that Mo (VI) is stabilized as MoO_4^{2-} in the outer layer of the film by the high electric field, leading to the deprotonation of OH^- within the film to supply O^{2-} required for formation of a protective Cr_2O_3 inner layer [50]. According to the results of Lloyd et al [7], such a Cr/Mo segregation process is only observable on high-Cr alloys such as Alloy C-22 and C-2000.

The segregation of alloying elements in passive films is a well known phenomenon, and can be attributed to either preferential oxidation of one alloying element in the alloy or preferential dissolution of other elements from the film, or both [51]. The accumulation of Cu on the surface of Ni–Cr–Mo alloys has been previously observed by the authors but remains unexplained [11]. For 304 stainless steel (0.19 wt.% Cu) it was claimed that the preferential dissolution of Fe, Cr, Ni, Mn and Mo lead to a residual Cu film which inhibits steel dissolution [52], and the deposition of Cu on the surface of 316 sintered stainless steel (0.25–5.0 wt.% Cu) appeared to improve its corrosion resistance [53]. The beneficial effect of alloying with Cu was attributed to its stability when deposited Cu on an anodically oxidized surface. While the morphology of the deposited Cu on the surfaces of ferritic and austenitic steel was found to vary [54], a metallic Cu layer is proposed by most researchers [55]. However, the role of Cu in stainless steel remains undefined. The deposited Cu layer was found to dissolve as $CuCl_2^-$ in solutions of low pH and high Cl^- concentrations at sufficiently positive potentials, and its dissolution occurred at lower potentials as the Cl^- concentration increased [52,54].

The chemical state of the Cu layer on the surface of Alloy C2000 after polarization at 0 V (vs. Ag/AgCl in saturated KCl) is difficult to determine by XPS and ToF-SIMS, since Cu (II) species can be reduced to Cu (I) under X-ray exposure [48]. Thermodynamically, Cu (I) would be expected at 0 V (vs. Ag/AgCl in saturated KCl) [54,56], but the closeness of the BEs for Cu and Cu_2O makes their

Fig. 7. $Cr_2O_3^-/MoO_3^-$ (solid line) and $Cr_2O_3^-/CuO^-$ (dotted line) intensity ratios from ToF-SIMS sputtering profiles recorded on Alloy C-2000 after polarization at 0 V (vs. Ag/AgCl in saturated KCl) (pH 7, 44 h) at 22 °C (black), 50 °C (red) and 90 °C (blue). The vertical dashed and solid lines represent the locations of the peak $Cr_2O_3^-/CuO^-$ and $Cr_2O_3^-/MoO_3^-$ ratios at 22 °C, respectively. (For interpretation of the references to color in this figure legend, the reader is referred to the web version of this article.)

separation in XPS spectra difficult. The CuO and $Cu(OH)_2$ found on Alloy C-2000 by ToF-SIMS is likely due to ion interactions in the sputtering/analysis chamber of the instrument, and cannot be used to confirm the oxidation state of the Cu.

The evolution of passive film composition and structure of Ni–Cr–Mo alloys with temperature has not been previously characterized. Zadorozne et al. [57] studied the breakdown potentials for a number of Ni–Cr–Mo alloys using the PD-GS-PD technique [29] but did not investigate the influence of temperature. More recently the same technique was used to measure the influence of temperature on the initiation of crevice corrosion on a series (7) of Ni–Cr–Mo alloys [58]. In these experiments the potential of a multiple crevice assembly was monitored at an applied current of 30 μA for 40 h at a series of individual temperatures, and the initiation of crevice corrosion indicated by a sudden decrease in potential. The temperature at which crevice initiation occurred was considered the passive film breakdown temperature. For high Cr alloys, like the C-2000 used in this study, breakdown occurred for $T \geqslant 55$ °C, and the breakdown temperature increased to 75 °C as the Mo + W content of the alloy was increased.

Since these experiments were conducted on creviced electrodes at an applied current of 30 μA, conditions inside the crevice when film breakdown occurred would be acidified and any changes in film composition prior to breakdown cannot be totally attributed to temperature. However, Gray et al. [3] also identified the temperature range 50 °C to 90 °C as that over which a substantial increase in passive corrosion rate occurred, again under acidic conditions.

Although our experiments were conducted in neutral solutions, any significant changes in film composition also occurred within this temperature range. At 22 °C the bilayer structure of the passive film was confirmed with an inner barrier layer of Ni/Cr oxide and an outer hydroxide layer enriched in Mo and Cu. As the temperature was increased this structure was maintained up to 50 °C. The passive current measured at this temperature is only slightly greater than that measured at 22 °C consistent with the observations of Gray et al. [3] in acidic conditions. A loss of Cr content in the inner and of Mo content in the outer layers was observed, but this was accompanied by a significant increase in overall film thickness.

These two counterbalancing influences, an increase in overall thickness but a decrease in Cr/Mo content, would explain the observed minor influence of temperature on the passive current density over this temperature range (22 °C to 50 °C). When the temperature was increased to 90 °C, these two trends continue; the overall film becomes substantially thicker but significantly depleted in Cr/Mo. Despite this depletion in the two elements generally responsible for the maintenance of passivity, the passive current density increases by only a factor of 2 to 3. This minor increase can be attributed to a very substantial thickening of the inner layer oxide allowing passivity to be maintained despite loss of Cr and Mo.

Our results are consistent with those of Gray et al. [3] who found a similar lack of sensitivity of passive current to temperature on Ni–Cr–Mo alloys for temperatures up to 50 °C. At higher temperatures they claimed a slow increase in passive current with increasing temperature could be attributed to an increase in Cr solubility. Our results show this provides only a partial explanation which does not take into account the simultaneous increase in solubility of Mo and the ability of the thicker $NiO/Ni(OH)_2$ to maintain passivity. The common assumption that passivity can be viewed as controlled by the rate of film regrowth at the alloy/oxide interface in response to its chemical dissolution at the film/solution interface does not apply.

While enrichment of Cu in the outer regions of the film is enhanced at both 50 °C and 90 °C its influence, if any, on maintaining passivity remains to be elucidated.

5. Conclusions

The passive oxide films (0 V vs. Ag/AgCl in saturated KCl) on Alloy C-2000 at various temperatures were investigated by surface-sensitive AR-XPS and ToF-SIMS techniques. Consistent with previous results, the presence of a layered structure has been demonstrated in this study at low and mild temperatures in neutral solutions. All the surface analyses show consistently high levels of hydroxides in the outer layer compared to oxides in the inner layer, and Cu and Mo oxide/hydroxide are enriched in the outermost surface. This confirms that the enrichment of Cr (and Ni) oxides at the alloy/oxide interface, is the critical feature in achieving passivity, while, Mo (and Cu) oxides segregate to the oxide/solution interface.

As temperature increases, the film-growth process is enhanced and the thicknesses of both the outer hydroxide layer and inner oxide layer increase. Also, the Ni content of the film significantly increases, whereas the Cr and Mo contents decrease with increasing temperature. Cu becomes enriched in the outer regions of the film, especially at intermediate temperatures. An increasing loss of Cr_2O_3 in the inner layer was observed as the temperature increases, which becomes very significant at 90 °C, and the observed loss of Cr/Mo segregation in the film may eventually lead to passivity breakdown if the temperature is increased far enough.

References

[1] R. Rebak, Corrosion of non-ferrous alloys, I-Nickel-, Cobalt-, Copper-, Zirconium-, and Titanium-based alloys, in: M. Schutze (Ed.), Corrosion and Environmental Degradation, Wiley-VCH, vol. 11, 2000, pp. 69–111.

[2] P.L. Andresen, L.M. Young, G.M. Catlin, P.W. Emigh, G.M. Gordon, Stress-corrosion-crack initiation and growth-rate studies on titanium grade 7 and alloy 22 in concentrated groundwater, Metall. Mater. Trans. A 36A (5) (2005) 1187–1198.

[3] J.J. Gray, J.R. Hayes, G.E. Gdowski, B.E. Viani, C.A. Orme, Influence of solution pH, anion concentration, and temperature on the corrosion properties of alloy 22, J. Electrochem. Soc. 153 (3) (2006) B61–B67.

[4] J.J. Gray, J.R. Hayes, G.E. Gdowski, C.A. Orme, Inhibiting effects of nitrates on the passive film breakdown of alloy 22 in chloride environments, J. Electrochem. Soc. 153 (5) (2006) B156–B161.

[5] M.A. Rodríguez, R.M. Carranza, R.B. Rebak, Passivation and depassivation of alloy 22 in acidic chloride solutions corrosion, passivation, and anodic films, J. Electrochem. Soc. 157 (1) (2010) C1–C8.

[6] M.A. Rodríguez, R.M. Carranza, R.B. Rebak, Influence of halide ions and alloy microstructure on the passive and localized corrosion behavior of alloy 22, Metall. Mater. Trans. A 36A (5) (2005) 1179–1185.

[7] A.C. Lloyd, D.W. Shoesmith, N.S. McIntyre, J.J. Noël, Effect of temperature and potential on the passive corrosion properties of alloys C 22 and C 276, J. Electrochem. Soc. 150 (4) (2003) B120–B130.

[8] A.C. Lloyd, J.J. Noël, N.S. McIntyre, D.W. Shoesmith, Cr, Mo and W alloying additions in Ni and their effect on passivity, Electrochim. Acta 49 (17–18) (2004) 3015–3027.

[9] A.C. Lloyd, J.J. Noël, N.S. McIntyre, D.W. Shoesmith, The open-circuit ennoblement of alloy C-22 and other Ni–Cr–Mo alloys, JOM 57 (1) (2005) 31–35.

[10] D. Zagidulin, X. Zhang, J. Zhou, J.J. Noël, D.W. Shoesmith, Characterization of surface composition on alloy-22 in neutral chloride solutions, Surf. Interface Anal. 45 (2013) 1014–1019.

[11] X. Zhang, D. Zagidulin, D.W. Shoesmith, Characterization of film properties on the Ni–Cr–Mo alloy C-2000, Electrochim. Acta 89 (2013) 814–822.

[12] J.J. Gray, C.A. Orme, Electrochemical impedance spectroscopy study of the passive films of alloy 22 in low pH nitrate and chloride environments, Electrochim. Acta 52 (7) (2007) 2370–2375.

[13] D.D. MacDonald, A. Sun, N. Priyantha, P. Jayaweera, An electrochemical impedance study of alloy-22 in NaCl brine at elevated temperature: II. Reaction mechanism analysis, J. Electroanal. Chem. 572 (2004) 421–431.

[14] N. Priyantha, P. Jayaweera, D.D. Macdonald, A. Sun, An electrochemical impedance study of alloy 22 in NaCl brine at elevated temperature. I.Corrosion behavior, J. Electroanal. Chem. 572 (2004) 409–419.

[15] D.D. MacDonald, A. Sun, An electrochemical impedance spectroscopic study of the passive state on alloy 22, Electrochim. Acta 51 (2006) 1767–1779.

[16] M. Bojinov, P. Kinnunen, G. Sundholm, Electrochemical behavior of Nickel–Chromium alloys in a high-temperature aqueous electrolyte, Corrosion 59 (2) (2003) 91–103.

[17] M. Bojinov, A. Galtayries, P. Kinnunen, A. Machet, P. Marcus, Estimation of the parameters of oxide film growth on nickle-based alloys in high-temperature water electrolytes, Electrochim. Acta 52 (2007) 7475–7483.

[18] P. Jakupi, D. Zagidulin, J.J. Noël, D.W. Shoesmith, The impedance properties of the oxide film on the Ni–Cr–Mo alloy-22 in neutral concentrated sodium chloride solution, Electrochim. Acta 56 (17) (2011) 6251–6259.

[19] G.M.F.N. Gordon, Speller award lecture: corrosion considerations related to permanent disposal of high-level radioactive waste, Corrosion 58 (10) (2002) 811–825.

[20] D.S. Dunn, L. Yang, C. Wu, G.A. Cragnolino, Effect of inhibiting oxyanions on the localized corrosion susceptibility of waste package container materials, Mater. Res. Soc. Sympos. (2004) 33–38.

[21] S.D. Day, M.T. Whalen, K.J. King, G.A. Hust, L.L. Wong, J.C. Estill, R.B. Rebak, Corrosion behavior of alloy 22 in oxalic acid and sodium chloride solutions, Corrosion 60 (9) (2004) 804–814.

[22] D.D. Macdonald, G. Engelhardt, P. Jayaweera, N. Priyantha, A. Davydov, The deterministic prediction of localized corrosion damage to alloy C-22 HLNW canisters, Eur. Federat. Corros. Publ. 36 (2003) 103–117.

[23] B.A. Kehler, G.O. Ilevbare, J.R. Scully, Crevice corrosion stabilization and repassivation behavior of alloy 625 and alloy 22, Corrosion 57 (2001) 1042–1065.

[24] K.J. Evans, A. Yilmaz, S.D. Day, L.L. Wong, J.C. Estill, R.B. Rebak, Using electrochemical methods to determine alloy 22's crevice corrosion repassivation potential, JOM 57 (1) (2005) 56–61.

[25] D.S. Dunn, Y.M. Pan, K.T. Chiang, L. Yang, G.A. Cragnolino, X. He, The localized corrosion resistance and mechanical properties of alloy 22 waste package outer containers, JOM 57 (1) (2005) 49–55.

[26] V. Jain, D. Dunn, N. Sridhar, L. Yang, Effects of measurement methods and solution chemistry on the evaluation of the localized corrosion of candidate high-level waste container materials, Corrosion 2003, paper No. 03690, Houston, TX, NACE International.

[27] D.S. Dunn, L. Yang, Y.M. Pan, G.A. Cragnolino, Localized Corrosion Susceptibility of Alloy 22, Corrosion 2003, Paper No. 03697, Houston, TX, NACE International.

[28] R.B. Rebak, Factors Affecting the Crevice Corrosion Susceptibility of Alloy 22, Corrosion 2005, Paper No. 05610, Houston, TX, NACE International.

[29] A.K. Mishra, G.S. Frankel, Crevice corrosion repassivation of alloy 22 in aggressive environments, Corrosion 64 (11) (2008) 836–844.

[30] M.R. Ortíz, M.A. Rodríguez, R.M. Carranza, R.B. Rebak, Corroison 66 (10) (2010). 105002-105002-12.

[31] C.M. Giordano1, M.R. Ortíz, M.A. Rodríguez, R.M. Carranza, R.B. Rebak, Crevice corrosion testing methods for measuring repassivation potential of alloy 22, Corrosion Eng., Sci. Technol. 46 (2) (2011) 129–133.

[32] R.M. Carranza, M.A. Rodríguez, R.B. Rebak, Effect of fluoride ions on crevice corrosion and passive behavior of alloy 22 in hot chloride solutions, Corrosion 63 (5) (2007) 480–490.

[33] X. He, B. Brettman, H. Jung, Effects of test methods on crevice corrosion repassivation potential measurements of alloy 22, Corrosion 65 (7) (2009) 449–460.

[34] M.A. Rodríguez, R.M. Carranza, R.B. Rebak, Effect of potential on crevice corrosion kinetics of alloy, Corrosion 66 (1) (2010). 015007-015007-14.

[35] P. Jakupi, D. Zagidulin, J.J. Noël, D.W. Shoesmith, Crevice corrosion of Ni–Cr–Mo alloys, Electrochem. Soc. Trans. 3 (31) (2007) 259–271.

[36] P. Jakupi, J.J. Noël, D.W. Shoesmith, Intergranular corrosion resistance of $\Sigma 3$ grain boundaries in alloy 22, Electrochem. Solid- State Lett. 13 (3) (2010) C1–C3.

[37] P. Jakupi, J.J. Noël, D.W. Shoesmith, Crevice corrosion initiation and propagation on alloy-22 under galvanically-coupled and galvanostatic conditions, Corros. Sci. 53 (10) (2011) 3122–3130.

[38] P. Jakupi, J.J. Noël, D.W. Shoesmith, The evolution of crevice corrosion damage on the Ni–Cr–Mo–W alloy-22 determined by confocal laser scanning microscopy, Corros. Sci. 54 (2012) 260–269.

[39] P. Jakupi, F. Wang, J.J. Noël, D.W. Shoesmith, Corrosion product analysis on crevice corroded alloy-22 specimens, Corros. Sci. 53 (5) (2011) 1670–1679.

[40] Y. Ashida, L.G. McMillion, M.L. Taylor, The effect of temperature oscillation on the passive corrosion properties of alloy 22, Electrochem. Commun. 9 (5) (2007) 1102–1106.

[41] K.J. Evans, R.B. Rebak, Passivity of alloy 22 in concentrated electrolytes effect of temperature and solution composition, Electrochem. Soc. Proc. 13 (2002) 344–354.

[42] M.C. Biesinger, B.P. Payne, L.W.M. Lau, A. Gerson, R.S.C. Smart, X-ray photoelectron spectroscopic chemical state quantification of mixed nickel metal, oxide and hydroxide systems, Surf. Interface Anal. 41 (4) (2009) 324–332.

[43] L.G. McMillion, A. Sun, D.D. MacDonald, D.A. Jones, General corrosion of alloy 22: experimental determination of model parameters from electrochemical impedance spectroscopy data, Metall. Mater. Trans. A 36A (5) (2005) 1129–1141.

[44] B.S. Norgren, M.A.J. Somers, J.H.W. Dewit, Application of tougaard background subtraction to xps spectra of passivated Fe–17 Cr, Surf. Interface Anal. 21 (6–7) (1994) 378–381.

[45] M.C. Biesinger, B.P. Payne, A.P. Grosvenor, L.W.M. Lau, A.R. Gerson, R.S.C. Smart, Resolving surface chemical states in XPS analysis of first row transition metals, oxides and hydroxides: Cr, Mn, Fe, Co and Ni, Appl. Surf. Sci. 257 (7) (2011) 2717–2730.

[46] M.C. Biesinger, C. Brown, J.R. Mycroft, R.D. Davidson, N.S. McIntyre, X-ray photoelectron spectroscopy studies of chromium compounds, Surf. Interface Anal. 36 (12) (2004) 1550–1563.

[47] P.A. Spevack, N.S. McIntyre, Thermal reduction of molybdenum trioxide, J. Phys. Chem. 96 (1992) 9029–9035.

[48] N.S. McIntyre, S. Sunder, D.W. Shoesmith, F.W. Stanchell, Chemical information from XPS—applications to the analysis of electrode surfaces, J. Vac. Sci. Technol. 18 (3) (1981) 714–721.

[49] A. Schneider, D. Kuron, S. Hofmann, R. Kirchheim, AES analysis of pits and passive films formed on Fe–Cr, Fe–Mo and Fe–Cr–Mo alloys, Corros. Sci. 31 (1990) 191–196.

[50] C.R. Clayton, Y.C. Lu, A bipolar model of the passivity of stainless steel: the role of Mo addition, J. Electrochem. Soc. 133 (12) (1986) 2465–2473.

[51] L. Zhang, D.D. Macdonald, Segregation of alloying elements in passive systems—I. XPS studies on the Ni–W system, Electrochim. Acta 43 (18) (1998) 2661–2671.

[52] K. Ogle, J. Baeyens, J. Swiatowska, P. Volovitch, Atomic emission spectroelectrochemistry applied to dealloying phenomena: I. The formation and dissolution of residual copper films on stainless steel, Electrochim. Acta 54 (22) (2009) 5163–5170.

[53] D. Itzhak, P. Peled, The effect of Cu addition on the corrosion behaviour of sintered stainless steel in H_2SO_4 environment, Corros. Sci. 26 (1) (1986) 49–54.

[54] T. Ujiro, S. Satoh, R.W. Staehle, W.H. Smyrl, Effect of alloying Cu on the corrosion resistance of stainless steels in chloride media, Corros. Sci. 43 (11) (2001) 2185–2200.

[55] M. Asawa, A. Devasenapathi, M. Fujisawa, Effect of corrosion product layer on SCC susceptibility of copper containing type 304 stainless steel in 1 M H_2SO_4, Mater. Sci. Eng., A 366 (2) (2004) 292–298.

[56] Marcel. Pourbaix, Atlas of Electrochemical Equilibria in Aqueous Solutions, Pergamon Press, Cebelcor, Brussels, 1966.

[57] N.S. Zadorozne, C.M. Giordano, M.A. Rodríguez, R.M. Carranza, R.B. Rebak, Crevice corrosion kinetics of nickel alloys bearing chromium and molybdenum, Electrochim. Acta 76 (2012) 94–101.

[58] A.K. Mishra, D.W. Shoesmith, Effect of Alloying Elements on Crevice Corrosion Inhibition of Nickel–Chromium–Molybdenum–Tungsten Alloys under Aggressive Conditions: An Electrochemical Study, in press.